Construction and Building Materials 392 (2023) 131771

Contents lists available at ScienceDirect

Construction and Building Materials

journal homepage: www.elsevier.com/locate/conbuildmat

Assessment of the tensile behavior of twisted steel connectors for masonry retrofitting

Sara Cattaneo [a,b,*], Manuela Scamardo [a]

[a] Department of Architecture, Built Environment and Construction Engineering, Politecnico di Milano, 20133 Milan, Italy
[b] Construction Technologies Institute, Italian National Research Council (ITC-CNR), 20098 San Giuliano Milanese, Italy

ARTICLE INFO

Keywords:
Masonry
Retrofitting
Twisted steel connectors
Pull-out test

ABSTRACT

The paper presents an experimental investigation on the tensile behavior of twisted stainless-steel bars considering different parameters that could affect their performance, namely the bar diameter (8, 10, 12 mm), the embedment depth, the position within the wall (installed into brick or in a T-mortar joint), the strength of the masonry and the type of loading (monotonic or cyclic load). Experimental results showed very good performance with reliable results associated to low coefficient of variation of the loads and very limited damage of the base material. The load–displacement curves showed a good ductility, an excellent superposition between monotonic and cyclic tests and an extended plateau at ultimate load. Among the different investigated parameters, the position within the wall was the most influential one, with higher loads associated to mid-brick location of the bar. Finally, based on the experimental results a user-friendly equation is proposed to predict the ultimate tensile load.

1. Introduction

The historical building heritage in Italy predominantly consists of unreinforced masonry structures. If on the one hand these buildings are characterized by a good resistance to vertical loads, on the other side, the resistance to horizontal loads, both in-plane and out of plane, is limited in the absence of good box-like behavior, as proved by the extensive damage observed during the most recent seismic events in Italy and worldwide [1–3].

Over the past decades, many efforts have been made to study and develop several retrofitting techniques to improve the resistance under horizontal loads [4–7]. For common buildings without specific historical value (mostly residential housing), traditional techniques, often invasive, are still very common [8–11]. Nevertheless, for valuable historical buildings and monuments, reversible, compatible, and non-invasive strengthening techniques are required by public authorities to keep any permanent effect to a minimum [12]. In the last years, the most common solutions used to improve walls transverse connections were connectors (steel or fiber reinforced polymers bars) inserted into a predrilled hole injected with grout or adhesive [13–15]. More recently, twisted stainless steel bars used with or without adhesives (dry application) have become very popular for both, crack stitching and to improve orthogonal connections between structural elements [16–19]. Predominantly, they are used without adhesives. The system as dry application typically requires a pilot hole (with a prescribed diameter smaller than the outer diameter of the bar) in which the twisted bar is easily inserted with a special mandrel. This technique has several advantages versus classical connectors using injection materials. First, it does not require any adhesive or grout, leading to a more compatible, reversible and sustainable solution. Second, the installation is very easy and quick, without specialized workforce, resulting in a reliable connection and in addition meaning that it also has economic advantages. Due to these reasons, these bars are commonly used and are becoming the preferred technique in case of historical buildings, where the reversibility of the strengthening technique is of primary importance. However, despite the spread in practical cases, there is a lack of knowledge of the overall behavior. In particular, they are often used to improve the strength of orthogonal connections. On the other hand, only few studies are available in literature on this topic. Moreira et al. [16] studied the pull-out behavior in mortar investigating the effects of the bar diameter, the embedment length and the diameter of the pre-drilled hole. They highlighted that the latter parameter has a strong influence on the final results, with improved strength with smaller holes. In addition, they noticed that with a hole diameter slightly lower than the

* Corresponding author.
E-mail addresses: sara.cattaneo@polimi.it (S. Cattaneo), manuela.scamardo@polimi.it (M. Scamardo).

https://doi.org/10.1016/j.conbuildmat.2023.131771
Received 16 February 2023; Received in revised form 28 April 2023; Accepted 10 May 2023
Available online 9 June 2023

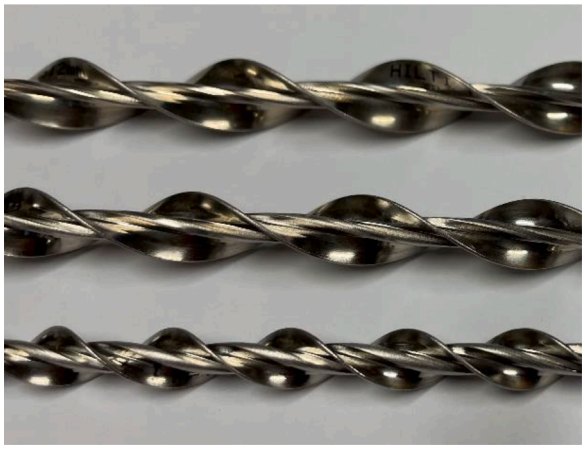

Fig. 1. Twisted bars.

bar diameter (difference of 2 mm) the larger rebar (10 mm) exhibited higher strength than smaller bar (8 mm), while the opposite behavior (higher strength of the 8 mm bar) was observed in case of smaller hole (4 mm smaller than the bar diameter). Gentilini et al. investigated first the influence of the substrate [17], performing several tests on different types of bricks, then carrying out pull-out tests of twisted bars installed in mortar cylinders [18]. They highlighted the importance of the mechanical characteristics of the substrate on the final performances, not only in terms of maximum load but also in terms of the post-peak behavior. In strong and stiff substrate, they found a plateau in the load–displacement curves, which was absent in weak and soft material. They also performed some cyclic tension tests and did not detect degradation due to cycling. In addition, thanks to the 3D scanning, they noticed a different penetration in soft and strong substrate during the installation and a certain untwisting of the bar in the latter during extraction.

In summary, the literature review shows that the geometry of the bar and of the hole plays a crucial role since the load-transfer mechanisms are those typical of a screw: by shape, thanks to the mechanical interlock of the wings of the bar in the base material, and by friction between the lateral surface of the bar and the hole.

Although to properly assess the behavior in practical applications also the shear performances should be studied, this paper focuses on the tensile strength in order to be able to design reinforcement of orthogonal wall connections.

This paper aims at investigating some crucial parameters that can affect the final behavior under axial loading starting from the results of an experimental program [20]. In particular, the twisted bars were installed in walls (considering two different strength) to account for the actual behavior into the masonry, whereby the tests were divided in two main groups considering installation in the middle of the brick or in the T-joint of the mortar layers (intersection of vertical and horizontal joints). Other parameters considered were the bar diameter, the embedment length, the orientation. In addition to monotonic tension tests, cyclic tests at different displacement level were performed. Finally, an equation for prediction of the ultimate tension resistance on the basis of geometric features of the bar and mechanical properties of the base materials is proposed.

2. Materials and methods

2.1. Specimen geometry and materials

The experimental research focused on the tensile behavior of twisted stainless-steel bars Hilti Heli-Brick (AISI 304) [21] used for retrofitting of masonry structures (Fig. 1).

The experimental campaign considered three bar diameters (8, 10, 12 mm). The mechanical properties of the twisted bars declared by the manufacturer are reported in Table 1. The Young's modulus declared by the manufacturer is higher than 122 GPa for all diameters.

Table 1
- Geometrical and mechanical properties of twisted bars "Heli-Brick" declared by the manufacturer [21].

Nominal drill bit diameter (mm)	Outer diameter (mm)	Nominal section (mm^2)	Tensile rupture load (kN)	Yielding load (kN)	Rupture Elongation (%)
5	8	10.4	12.0	10.8	4.8
6	10	12.9	16.0	13.4	5.7
8	12	15.1	18.9	16.1	–

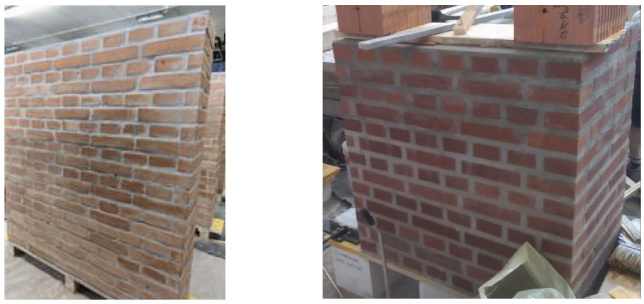

(a) (b)

Fig. 2. Weak (a) and strong (b) walls.

Table 2
Geometrical and mechanical properties of masonry specimens.

Masonry type	Joint thickness (mm)	Brick size (mm)	Compressive strength (MPa)	
			Brick	Mortar
Weak	12	250x120x50	25	5
Strong	16	250x120x60	34	8

The twisted bars were installed with a device provided by the manufacturer into pre-drilled holes of 5 mm, 6 mm and 8 mm for bar of diameters 8 mm, 10 mm and 12 mm, respectively. The embedment length varied depending on the test program. The holes were cleaned by blowing compressed air through an air nozzle (CAC - Compressed Air Cleaning) along the embedment depth at least three times.

To represent actual site conditions in the analysis, two types of masonry walls were built characterized by different mechanical characteristics. The "weak" (W) walls (Fig. 2a) were made of solid bricks (size 250 × 120 × 50 mm with nominal compressive strength of 18 MPa and actual strength around 25 MPa, tested according to [22]) and with a masonry mortar M2.5 with actual strength of 5 MPa. The "strong" (S) walls (Fig. 2b) were made of solid bricks (size 250 × 120 × 60 mm with nominal compressive strength of 18 MPa and actual strength around 34 MPa, tested according to [22]) and with a masonry mortar M5 with actual strength of 8 MPa (tested according to [23]). All walls were constructed using the English bond pattern. The "weak" walls had a size of 1290 × 1290 × 250 mm (joint thickness 10 mm) and the "strong" walls of 1000 × 1000 × 600 mm (joint thickness 20 mm). The main specimen properties are summarized in Table 2.

2.2. Test set-up

Fig. 3a shows a schematic drawing of the test set-up. The specific shape of twisted bar does not fit with usual clamping systems, therefore some trial tests were performed to evaluate the effectiveness of different clamping systems. At first, a wedge system was used, resulting in

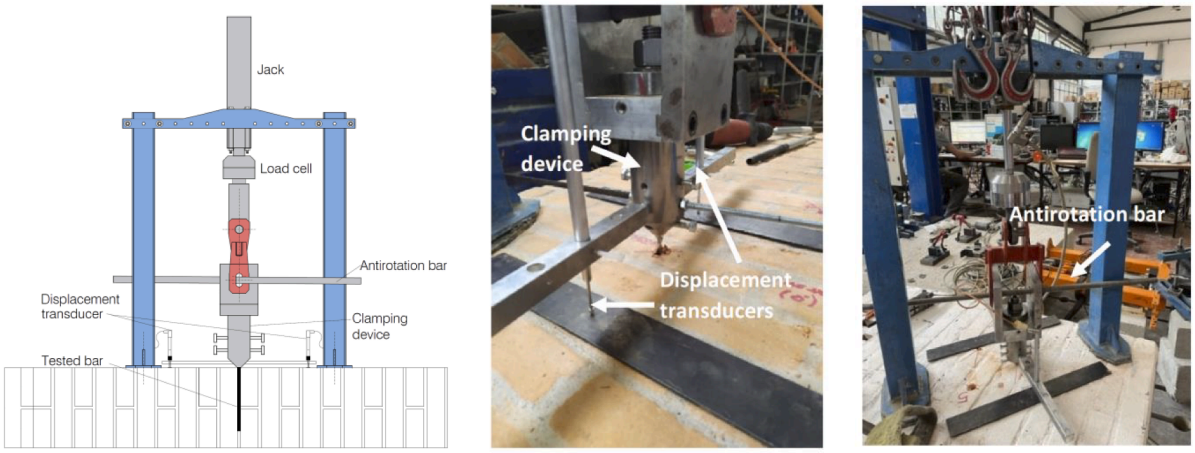

Fig. 3. Test set-up (a) and detail of the clamping device (b) and anti-rotation bar (c).

rotation of the twisted bar during the test. A phenomenon also being reported by other researchers [17]. As consequence, a special clamping device (Fig. 3b) was constructed featuring a horizontal bar which prevents the rotation (Fig. 3c). The clamping device consists of a steel cylinder with an inner hole (diameter of 12 mm). The cylinder had side holes to insert screws to clamp the twisted bar. The lateral holes had a spacing such as to grip the bar in the central section avoiding interference with the wings of the bar itself.

Unconfined tensile tests were performed with a test rig equipped with a 25 kN load cell and with two LVDTs (gage length 100 mm) placed symmetrically to the anchor axis, attached to the clamping system at 20 mm from the wall surface (Fig. 3a). The tests were displacement controlled and monitored with the MOOG system.

2.3. Test protocol and test plan

The test plan overall consisted of 91 tests. The main considered parameters were: (i) bar diameter (8, 10, 12 mm); (ii) wall strength (two different bricks and two different mortar strengths); (iii) embedment length (100, 200 and 400 mm); (iv) position of connectors (F-face of the wall or S-side of the wall and M−middle of the brick or in the T-joint mortar position); (v) orientation (0° and 45°).

The test program featured both monotonic (63) and cyclic tests (26). The cyclic tests considered three cycles at each displacement level. The levels were increased as follows: 0.25, 0.5, 1.0, 2.0, 3.5, 5, 7, 9, 11, 14, 17, 20, 25, 30, 40, 50, 60 mm. Since the tests showed very high residual displacements, additional cyclic tests were performed using compression forces while unloading to obtain displacements equal to zero.

This last procedure was performed on all diameters, while the cyclic tests with residual displacements were performed only on 12 mm diameter.

Each test was properly coded as follows: HExx (Helicoidal bar of size xx) - type of wall (Weak: W; Strong: S) - position (Face: F; Side: S) - position within the wall (Middle of the brick: M; T-joint: TJ) - orientation angle (0°, 45°H - horizontal or 45°V - vertical) - embedment length. The cyclic test with residual displacement were additionally coded with “C” at the end, while for the cyclic tests without residual displacement “CC” was added. In general, 3 tests per series were performed except for the case where the coefficient of variation of the load was higher than 15%, in which case the number of tests was increased up to 5.

Tests performed on 12 mm bar in the weak wall with embedment length equal to 200 mm and orientation equal to 0° are taken as reference. So, when part of the code is omitted in the following, these reference values are assumed.

A sketch of the position of the twisted bars within the walls is shown in Fig. 4.

3. Experimental results and discussion

Table 3 summarizes the obtained results for each cluster of tests in terms of average ultimate load (N_m) and corresponding coefficient of variation (v). The test identification explained above is applied.

All tests showed connector pull-out failure, except in some cyclic tests without residual displacements, where steel failure was observed because of the cyclic buckling (see next sections). It is worth noting that the damage to the masonry was extremely limited. In most cases the pull-out of the bar did not cause any damage except the hole and some dust (Fig. 5a-5e), while in other cases the damage was limited to few centimeters around the hole (e.g. up to 4–5 cm as shown in Fig. 5f).

The influences of the varied parameters are discussed in the next sections.

3.1. Influences of the position within the wall and of the wall strength

The experimental evidence showed that the position of the bar within the wall was of primary concern. In particular, the bars installed in the middle of the brick (M−position) exhibited higher strengths with lower coefficients of variation and a more ductile behavior compared to bars installed in the T-joint position. The mechanical responses of bars with diameter 12 mm (example presented in Fig. 6) showed that the ones installed in the middle of the brick exhibited a long plateau (Fig. 6a), while the ones installed in the T-joint exhibit a more pronounced softening branch independent of their inclination (Fig. 6b, 6c, 6d).

The bars oriented at 45° exhibited higher scatter, probably because they met several layers (brick/mortar- Fig. 4a, yellow and purple bars) and some inhomogeneities of the material affected the results. A similar behavior was observed for diameter 10 mm, while diameter 8 mm was different (Fig. 7). Indeed, the 8 mm bar presented a very high strength in the TJ-position (Fig. 7b and Table 3) and a very limited load plateau at about the same level than the other sizes when installed in the middle of the brick.

This apparently deviating behavior may be explained since the installation in the middle of the brick or in the T-joint was not always representing exactly the same conditions. Indeed, depending on the embedment length, bars installed in the middle of the brick can also include regions located in the mortar, when crossing one or more mortar joints (between two rows of bricks; see Fig. 4). Also, inclined bars

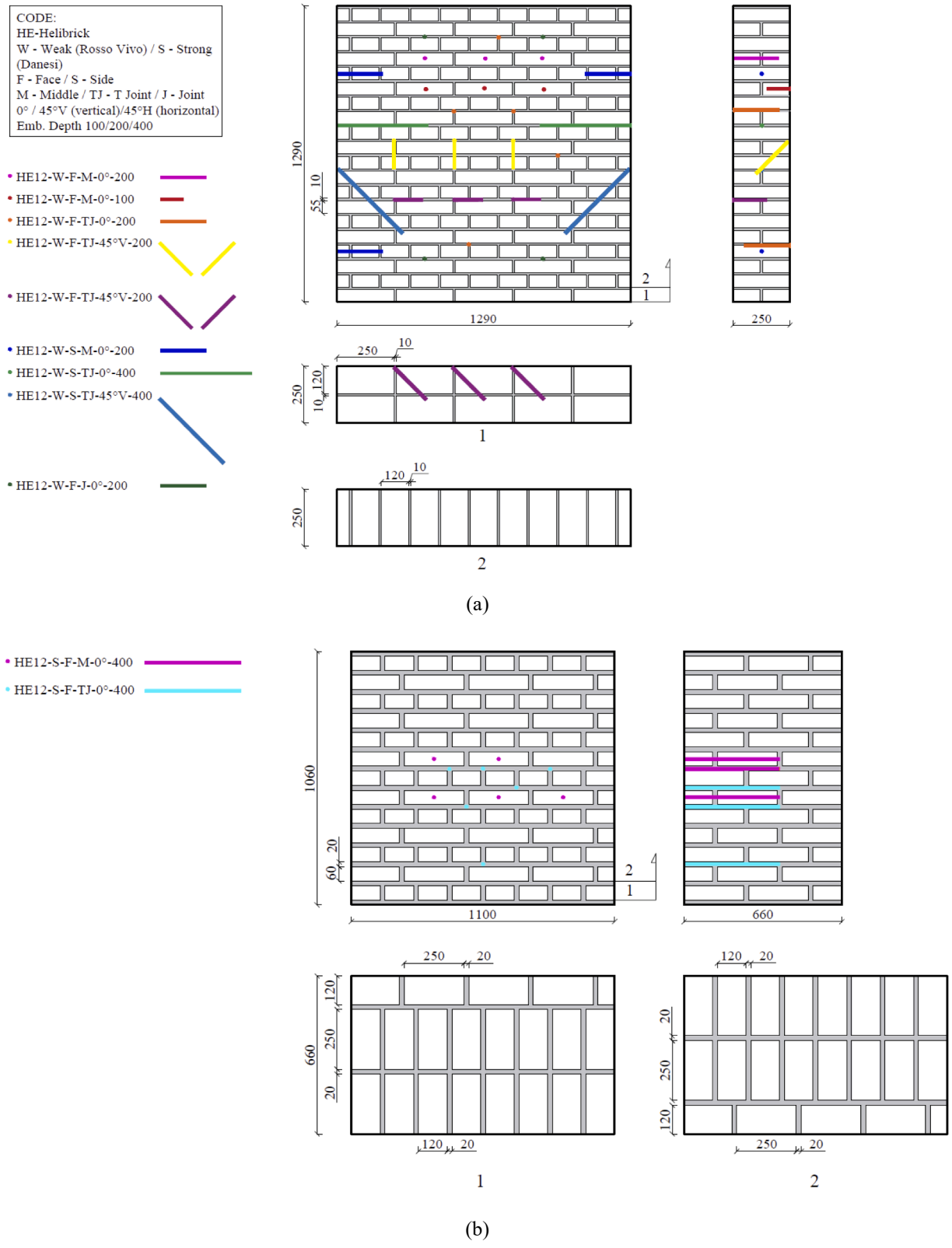

Fig. 4. Position of the twisted bars in the (a) weak wall and (b) strong wall.

installed in the T-joint can involve brick units (Fig. 4). In addition, although in all cases the drill diameter bit was smaller than thickness of the joint (10 mm in the weak wall), the 12 mm bar had a small portion embedded into the brick and the 10 mm bar was at least nominally in contact with the adjacent bricks. On the other side, the 8 mm bar was completely embedded into the mortar and could exhibit a higher strength due to the confinement of the surrounding bricks.

No specific differences, for the considered case, were observed in tests performed on the side and on the face of the wall (e.g., for the 12 mm bar 6.84 kN for HE12-W-F-M−0−200 vs 7.03 kN for HE12-W-S-

Table 3
Test results.

Test denomination	Embedment length (mm)	Wall type	Orientation (°)	N_m (kN)	v(N) %	N_m (kN)	v(N) %	N_m (kN)	v(N) %
HE12-W-F-M−0−100	100	Weak	0	5.5	3.2%				
HE12-W-F-M−0−200	200	Weak	0	6.8	5.1%	6.5	12.3%	5.9	19.1%
HE12-W-F-M−0−200−CC	200	Weak	0	6.8	1.7%				
HE12-W-F-M−0−200−C	200	Weak	0	5.2	6.8%				
HE12-W-S-M−0−200	200	Weak	0	7.0	3.6%				
HE12-W-F-TJ-0–200	200	Weak	0	5.3	4.4%	5.2	20.7%		
HE12-W-F-TJ-0–200-CC	200	Weak	0	3.9	11.1%				
HE12- W-F-TJ-0–200-C	200	Weak	0	6.4	2.0%				
HE12-W-F-TJ-M−45H−200	200	Weak	45H	5.3	16.2%	5.5	7.7%		
HE12 W-F-TJ-M−45 V-200	200	Weak	45 V	5.7	9.1%				
HE12 S-F-M−M−0−400	400	Strong	0	8.2	3.5%	7.7	9.0%	7.4	9.2%
HE12-S-F-TJ-M−0−400	400	Strong	0	7.2	8.4%				
HE12-W-S-TJ-M−0−400	400	Weak	0	6.6	4.9%	7.1	8.9%		
HE-12-W-S-TJ-45 V-400	400	Weak	45 V	7.6	4.2%				
HE10-W-F-M−0−200	200	Weak	0	5.2	4.8%	5.0	7.0%	4.4	25.9%
HE10-W-F-M−0−200−CC	200	Weak	0	4.9	8.9%				
HE10-W-F-TJ-0–200	200	Weak	0	4.9	4.6%	4.1	33.8%		
HE10 W-F-TJ-0–200-CC	200	Weak	0	3.3	44.6%				
HE8-W-F-M−0−200	200	Weak	0	5.5	17.7%	5.4	12.3%	5.5	17.9%
HE8-W-F-M−0−200−CC	200	Weak	0	5.3	6.2%				
HE8-W-F-TJ-0–200	200	Weak	0	6.6	9.2%	5.5	23.3%		
HE8-W-F-TJ-0-200CC	200	Weak	0	4.4	7.3%				
HE8-W-S-M−0−400	400	Weak	0	8.2	14.2%	6.7	29.4%		
HE8- W-S-TJ-0–400	400	Weak	0	5.8	32.2%				

Fig. 5. Examples of damage of the base material: during the test (a-b), for close bars (c), in the brick (d), in the T-joint (e) and around the hole (f).

M−0−200).

Overall, the strength of the wall (brick and/or masonry mortar) appeared to have a positive effect on the ultimate load (Table 3, diameter 12 with $h_{ef} = 400$ mm). For the two series installed orthogonally to the wall in the T-joint, the mean resistances increased from 6,6 kN (weak wall) to 7,2 kN (strong wall). For the inclined location (HE-12-W-S-TJ-400–45 V), where parts of bricks were involved, the mean resistance further increased to 7,6 kN (weak wall) and the highest value was 8,2 kN obtained at mid brick location of the strong wall.

3.2. *Influence of the bar diameter*

As already pointed out in the previous section, the bar diameter influenced the overall response. However, a direct relationship between

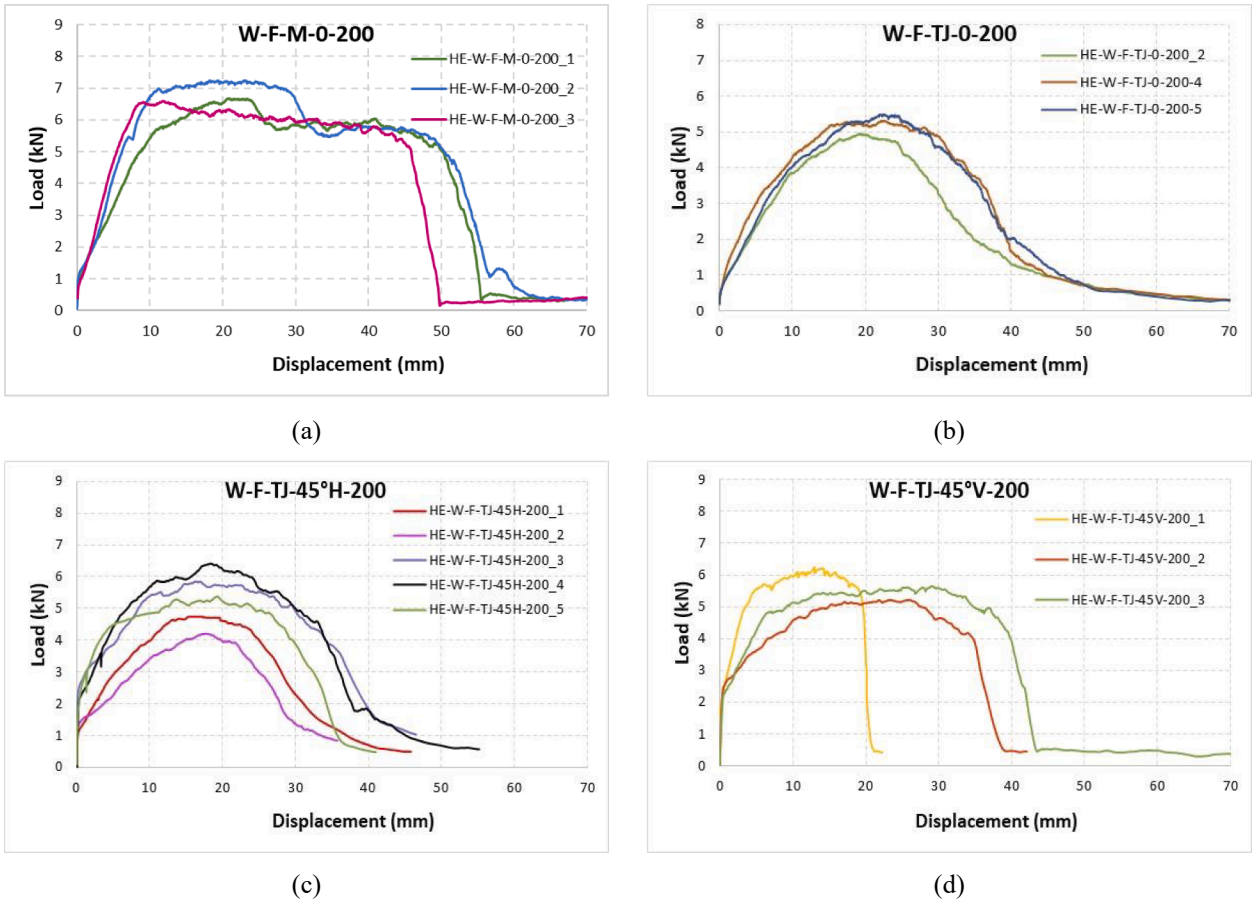

Fig. 6. Load-displacement curves – effect of the position (diameter 12 mm; h_{ef} = 200 mm): (a) in brick 0° oriented, (b) T-joint 0° oriented, (c) in T-joint 45° horizontally inclined and (d) in T-joint 45° vertically inclined.

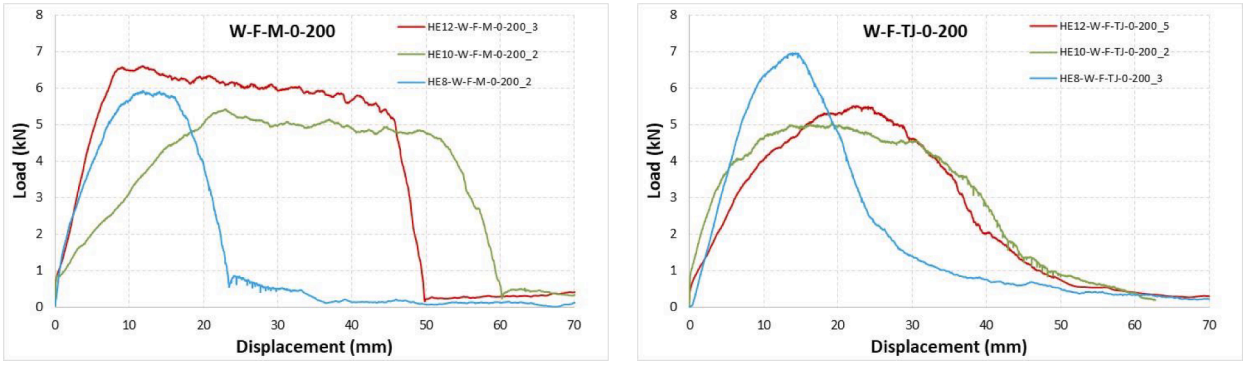

Fig. 7. Load-displacement curves for different bar diameter in the brick (a) and in the T-joint (b).

bar diameter and maximum load could not be found. Indeed, the 10 mm bar showed the lowest performances of all 3 diameters both in the middle of the brick and in the T-joint (Fig. 7). This behavior can be explained by the geometry of the bar in combination with the installation parameters. In particular, the bars had different cross-sections (specifically the "wing" geometry but similar core geometry), a different thread pitch (helicoidal path) and a different nominal drill bit diameter (see Table 1). This suggested how the combination of these parameters led to a critical behavior of the 10 mm bars, as observed in [16].

In summary, looking also at the coefficients of variation of the ultimate loads (Table 3), the 12 mm bar showed the best performance with the highest resistances and a more reliable overall response.

3.3. *Influence of the embedment depth*

The effect of the embedment depth was investigated for the bar diameters 8 and 12 mm in weak walls. A clear increase of the maximum load was detected (Fig. 8), although it was not proportional to the increase of the embedment depth. The behavior was similar whatever the orientation (0° or 45°).

In the T-joint, the 8 mm bar showed an opposite behavior with a

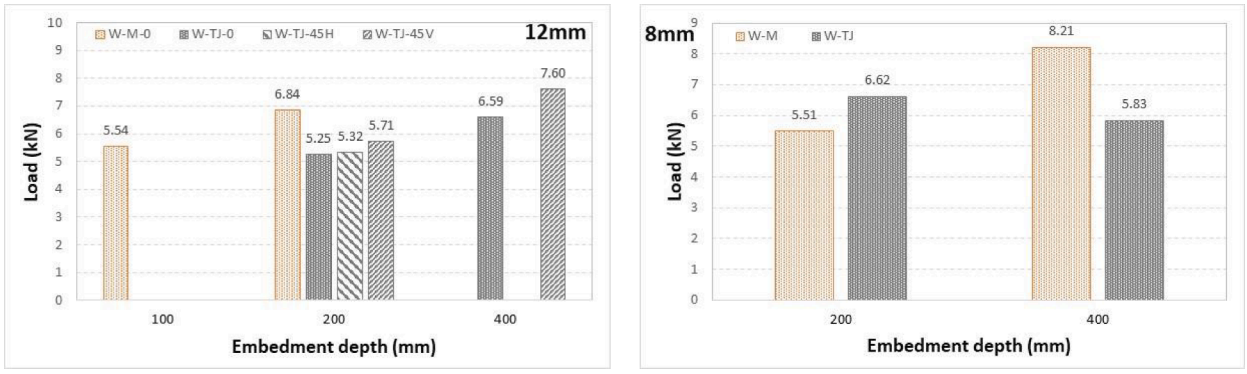

(a) (b)

Fig. 8. Maximum load as a function of the embedment depth in weak walls for 12 mm (a) and 8 mm (b).

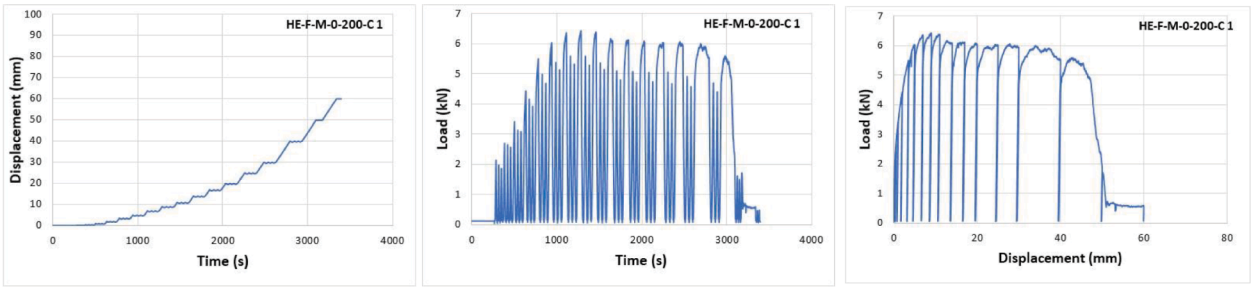

(a) (b) (c)

Fig. 9. Results of cyclic test with residual displacement for Heli-Brick size 12, h_{ef} = 200 mm, at mid-brick location of weak wall: displacement vs time (a), load vs time (b) and load vs displacement (c) curves.

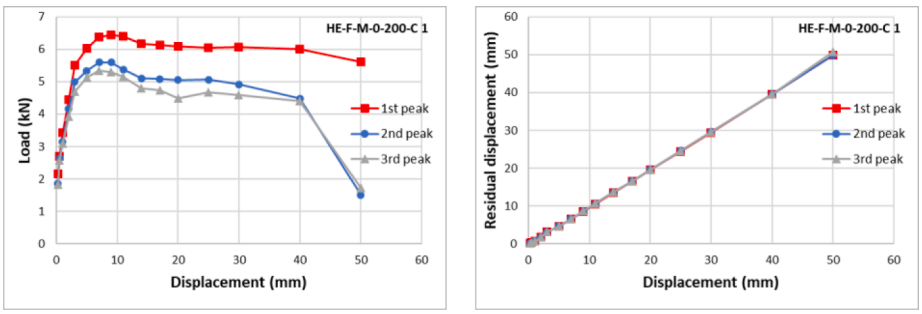

(a) (b)

Fig. 10. Peak load (a) and residual displacement (b) at each cycle for Heli-Brick size 12, h_{ef} = 200 mm, at mid-brick location of weak wall.

lower load for the higher embedment length. It must be remarked that, in this series, some problems were encountered during installation due to mortar debris settling in the borehole. The execution of the cleaning procedure with deep embedment depth was difficult due to the small diameter of the hole. This result underlines the importance of a well working cleaning procedure for the realization of a reliable connection [24].

3.4. *Influence of the type of loading*

In addition to the monotonically loaded quasi-static tests, the behavior of the twisted bar was investigated under displacement controlled cyclic load. Three cycles at each displacement level (see §2.3) were performed. Cyclic tests with residual displacement were conducted only for the diameter 12, while, for all diameters, tests without residual displacement were performed since they were regarded more representative of actual cases under seismic events (e.g., hammering of two adjacent elements).

Fig. 9 presents the results of a cyclic tension tests with residual displacement for size 12 in terms of displacement vs time (Fig. 9a), load vs time (Fig. 9b) and load vs displacement (Fig. 9c). It is evident that very high residual displacements were detected mainly after each first cycle. This can be seen by the "vertical" lines in Fig. 9c.

Fig. 10 shows the peak load (a) and the residual displacement (b) associated to each cycle of one test as example. A higher peak load in the first cycle of each displacement step with a load degradation in the following two cycles were detected. However, the decrease is significantly smaller between the second and third cycle than between the first and second, indicating an asymptotic behavior. The residual displacement showed a linear increasing trend with increasing displacement

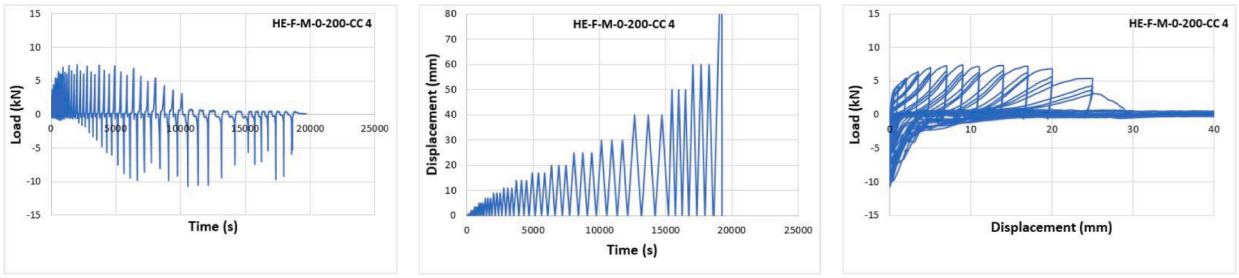

Fig. 11. Results of cyclic test without residual displacement for Heli-Brick size 12, h_{ef} = 200 mm, at mid-brick location of weak wall: displacement vs time (a), load vs time (b) and load vs displacement (c) curves.

Fig. 12. Twisted bar in compression (a) and failure in tension (b).

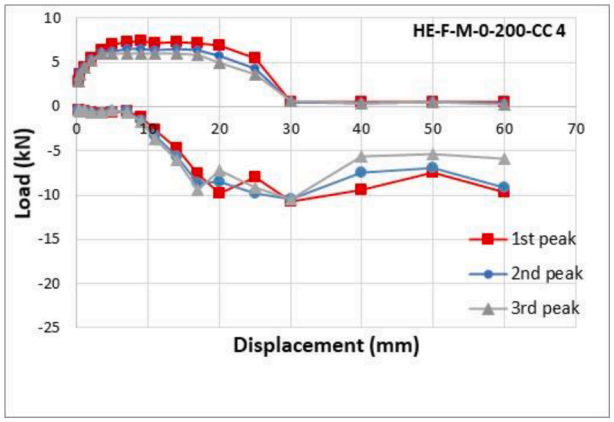

Fig. 13. Peak loads at each cycle for example with Heli-Brick size 12, h_{ef} = 200 mm, at mid-brick location of weak wall.

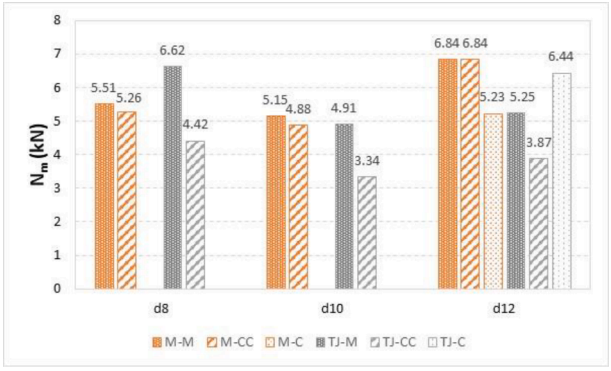

Fig. 14. Average peak loads for monotonic (M), cyclic with residual displacement (C), cyclic without residual displacement (CC) for each diameter and position (M or TJ).

levels but there was no significant difference between the three different cycles at each level. All tests, whatever the position within the wall, exhibited similar behavior [20].

The above-described cyclic tests were repeated, for all diameters, with the unloading branch until zero displacement. The results for size 12 are shown in Fig. 11.

Before the application of compressive load, the behavior of the bar in tension resulted similar to the one observed for cyclic tests with residual displacement), both in terms of load and in terms of high residual displacements. By decreasing the displacement to reach the original position, at first the bar moved without carrying load, then the bar underwent to compression (Fig. 12a). In some cases, the required compression load was very high (up to 25 kN) and, indeed, led to bar buckling. With increasing number of cycles, the axis of the bar and the axis of the hole misaligned and, due to the consequent eccentricity, in most of the tests, the bar bent and was pushed sidewards but not further into the drilled hole. In these cases, at the end of the test, the bar exhibited steel failure under tension load (Fig. 12b).

Fig. 13 shows the peak and the minimum load for each cycle as a function of the displacement. As for tests with residual displacement, a higher peak load in the first cycle of each displacement step was observed, while there was a degradation in the following cycles.

Fig. 14 presents the average peak load for each diameter, position (M or TJ) and type of load (monotonic -M, cyclic with residual displacement-C, cyclic without residual displacement-CC, performed

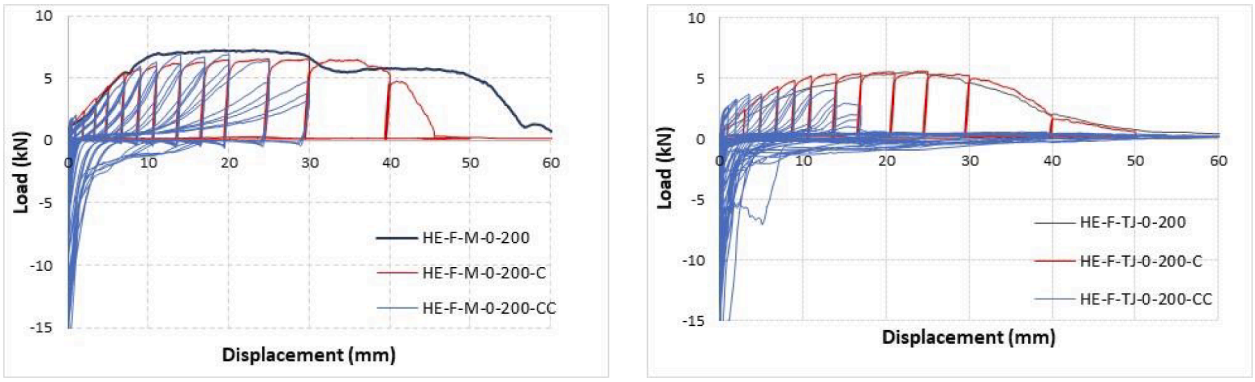

Fig. 15. Load-displacement curves for each type of load (monotonic, cyclic with residual displacement and cyclic without residual displacement) in the brick (a) and in the t-joint (b) for diameter 12.

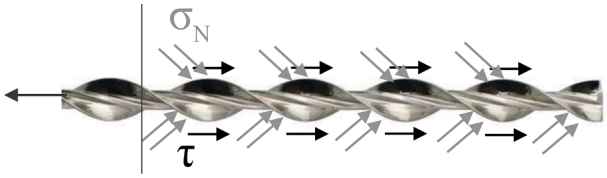

Fig. 16. Stresses along the bar.

only on diameter 12 mm) and Fig. 15 shows the load–displacement curves of monotonic and cyclic tests grouped by colors. In general, cyclic tests showed a good repeatability and similar results to those observed for monotonic tests. It can be noted that, for mid-brick location (Fig. 14, orange columns), there is a little difference between monotonic and cyclic loading in terms of peak load, except for the cases of cyclic test with residual displacement (only tests with size 12 available) where a reduced load was observed. An opposite behavior was observed in the T-joint (Fig. 14, grey columns), where a pronounced degradation due to cycling was observed. This is valid except for the case of diameter 12 mm, where higher ultimate tension loads were detected under cyclic load with residual displacement. However, it should be considered that these higher loads were associated to large displacements (Fig. 15).

4. Analytical model

The experimental campaign highlighted that several parameters affect the load carrying capacity of twisted bars. Nevertheless, from a practical point of view, the designer needs clear information to be able to use this technique in real application.

To this end, a user-friendly equation has been developed to predict the ultimate load in the different cases.

Twisted bars are inserted into a predrilled hole in the base material by hammering with a hammer drilling machine (without active rotation) using a specific setting tool. The tool allows for a rotation of the Heli-Brick during installation. Therefore, the resistant mechanisms are those typical of a screw: by shape, thanks to the mechanical interlock of the wings of the bar in the base material, and by friction between the lateral surface of the parts of the bar and the hole (Fig. 16).

In detail, the definition of the geometries involved (angles and areas) is challenging and, from a practical point of view, it is more convenient to consider a formulation that accounts for easily quantifiable parameters such as the outer diameter of the bar (d), the diameter of the drill hole (d_h), the pitch (p), the effective embedment length (h_{ef}) (Fig. 17). Indeed, due to the geometry of the spiral shaped bar (that beside the wings also features a twisted, almost rectangular core section), the effect of the lateral friction can be neglected. Thus, the carrying capacity of the bar could be evaluated considering the shape resistance of the wings of the bar that interlock with the base material. The effective area involved has a thickness equal to $t_w = (d\text{-}d_h)/2$ and a length equal to the total length of the two spiral wings along the effective embedment depth h_{ef} (Fig. 17).

To evaluate the length of the reacting area, the sketch of Fig. 18 can be considered. First, the length l along a pitch p can be calculated. Considering the radius r (Fig. 17):

$$r = (d_h + t_w)/2 \tag{1}$$

(at the middle of the wing), the length l can be easily evaluated:

$$l = \sqrt{(2\pi r)^2 + p^2} \tag{2}$$

Due to the geometry of the twisted bar along the pitch (2 wings), 2 l should be considered (Fig. 18) along the total height h_{ef}.

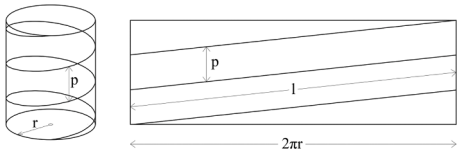

Fig. 18. Length l of the path.

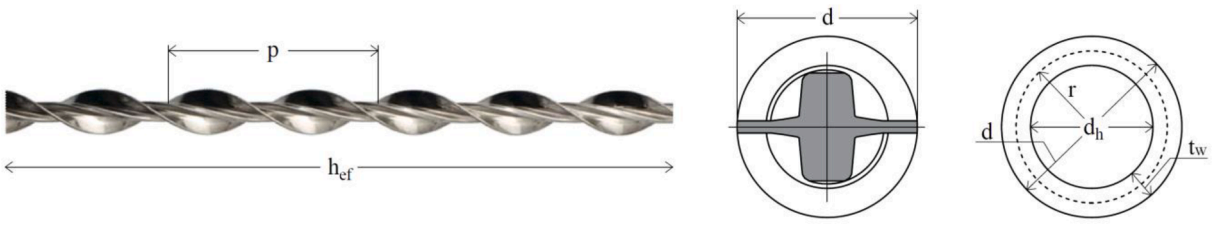

Fig. 17. Geometry of the twisted bar.

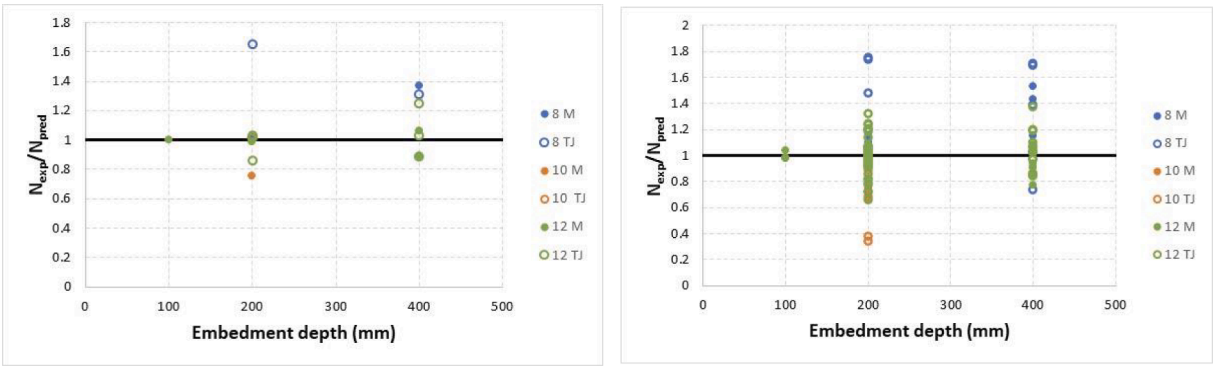

(a) (b)

Fig. 19. Experimental/predicted load ratio: considering only the monotonic tests for diameter 12 (a) and considering all values (b).

According to this approach, by considering Eq 1–2 to define the lateral surface of the wings, the ultimate load N_u can be evaluated as follows:

$$N_u = f_{bm} \cdot 2l \cdot \frac{h_{ef}}{p} \cdot t_w \cdot s = f_{bm} \cdot 2\sqrt{\pi^2 (d_h + t_w)^2 + p^2} \cdot \frac{h_{ef}}{p} \cdot t_w \cdot s \quad (3)$$

where f_{bm} is the base material strength and s is a parameter that accounts for the size effect and the non-uniform stress distribution along the bar.

The definition of the material strength f_{bm} is challenging because it depends on the position of the bar within the wall, so that either bricks or mortar joints or a combination of both with corresponding strength values can be involved.

In particular, depending on the position of the connection, the bar could be installed in different base materials. Up to four possible cases can be identified:

(i) the bar installed in the middle of one brick
(ii) depending on the embedment length and for deep installation, the bar installed in the middle of the outer bricks could cross one or more mortar joints and then penetrate one or more rear bricks, so the base material is a mix between brick and mortar
(iii) the bar installed in the joint has only mortar as base material
(iv) the bar installed in the joint which has a thickness lower than the outer bar diameter (e.g., bar diameter 12 mm and joint 10 mm) has both mortar and brick as base material since the external part of the wings of the bar is installed into the brick.

To consider the different positions within the wall, the base material strength can be defined as a combination of the two materials mortar and brick as follows (similar approach to that presented in [25]):

$$f_{bm} = c_1 \cdot f_m + c_2 \cdot f_b^{0.65} \quad (4)$$

where f_m and f_b are the mortar and brick compressive strength, respectively, while c_1 and c_2 are two geometrical parameters that account for the percentage of the depth into the mortar and into the brick (e.g., in the T-joint position (iii) $c_1 = 1$ and $c_2 = 0$, while in the middle of an outer stretcher brick $c_1 = 0.05$ and $c_2 = 0.95$ for 200 mm embedment length, as an intermediate mortar joint of 10 mm thickness is penetrated as well).

The parameters in equation (3) considers that, in case of long embedment depth, not the full anchor length contributes to the load transfer to the same extend; at the beginning of loading, only the first part (close to the base material surface) of the bar is fully activated, while the rear part is nearly unloaded. By increasing the load further, the undercut created in the base material in the first part (closer to surface) starts crushing, while the rear parts of the bar are getting more and more involved in the load transfer. Thus, especially for deep embedment, only subsequent portions of the bar contribute to the load carrying capacity at a time and not the entire embedded length.

To account for this behavior, for the parameter s an empirical decreasing function that considers this decline with h_{ef} (in mm) is introduced:

$$s = \left(\frac{200}{h_{ef}}\right)^{\left(k_1 + k_2 h_{ef} + k_3 h_{ef}^2\right)} \quad (5)$$

The parameters k_1, k_2 and k_3 were evaluated on the basis of the experimental results as follows: $k_1 = 0.574$; $k_2 = 0.001$; $k_3 = -7.63 \times 10^{-7}$.

These parameters were calibrated considering the average values of monotonic tests with size 12 mm in brick (M) and T-joint locations with

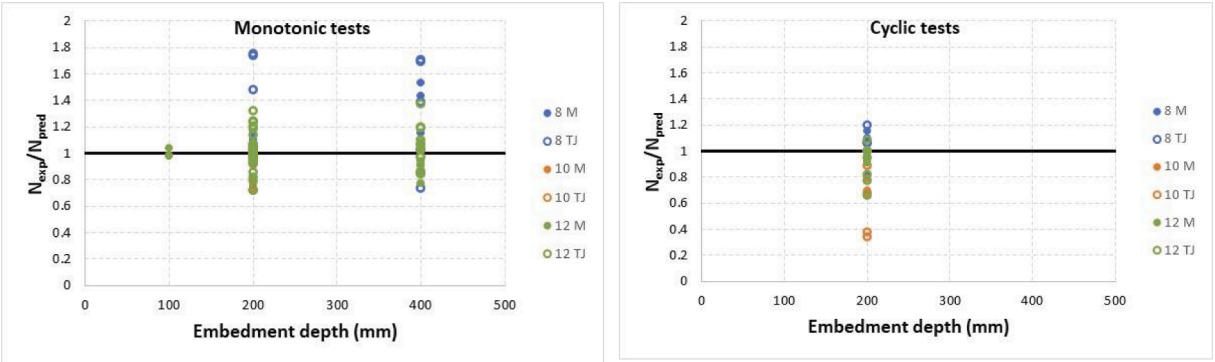

(a) (b)

Fig. 20. Experimental/predicted load ratio of monotonic (a) and cyclic (b) tests for different embedment depth.

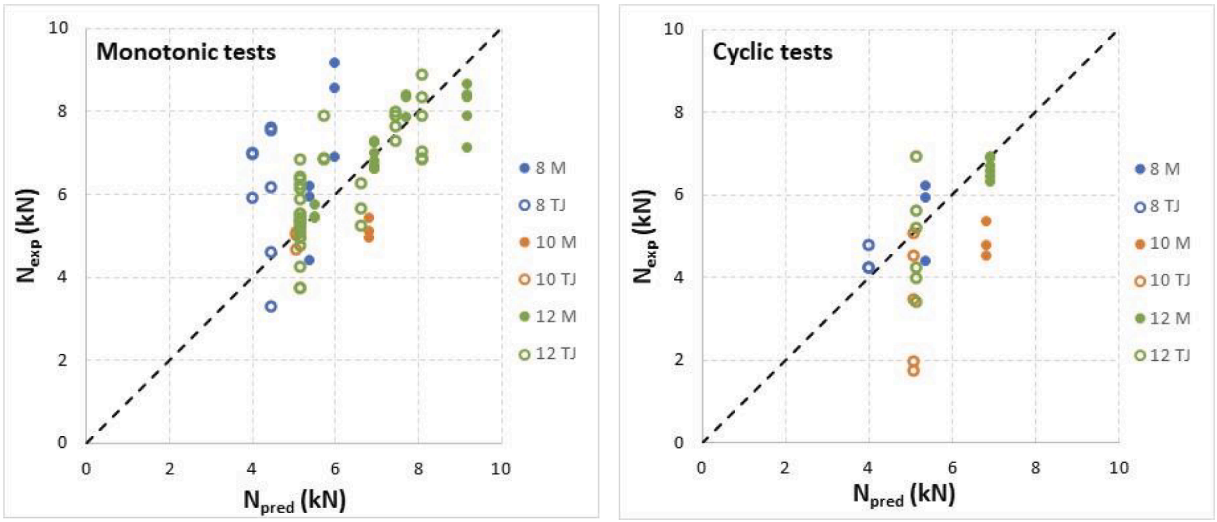

Fig. 21. Experimental/predicted load ratio of monotonic (a) and cyclic (b) tests.

200 mm and 400 mm embedment depth (Fig. 19a). The results of size 8 and 10 mm were not used for calibration to be able to assess the ability of the formula to predict their ultimate load. It can be noted that some outlier points (e.g., in series 8TJ and 10 M) are not well predicted. By considering all data including the cyclic test results (Fig. 19b), it can be noted that the formulation underestimates the results of diameter 8 and overestimates the results of diameter 10 whereas the diameter 12 is better predicted.

Indeed, the average safety factor γ_{ave} defined as the ratio between the experimental maximum load and the predicted one, is above 1 for diameter of 8 mm ($\gamma_{ave} = 1.12$ for 8 M and $\gamma_{ave} = 1.35$ for 8TJ), while it is below 1 for diameter 10 mm ($\gamma_{ave} = 0.73$ for 10 M and $\gamma_{ave} = 0.77$ for 10TJ). In the case of diameter 12 mm γ_{ave} results 0.98 and 0.99 in the brick and in the T-joint respectively.

By splitting the results of Fig. 19b between monotonic and cyclic tests (Figs. 20-21), it is observed that in monotonic tests the model clearly underestimates the load of the diameter 8 ($\gamma_{ave} = 1.19$), while in cyclic tests the load is overestimated for diameter 10 ($\gamma_{ave} = 0.71$ in the middle of the brick and $\gamma_{ave} = 0.75$ in the TJ position) and therefore in case of seismic loads an appropriate coefficient should be introduced.

In addition, it is suggested to adopt the approach presented in the seismic variant EAD 330076–01-0604-v01 [26] in a simplified way, considering the two parameters that take into account the difference in the peak load between monotonic and cyclic tests and the decay due to subsequent cycles. The European Document [26] is based on the assumption that cyclic tests usually reached lower maximum load with respect to the corresponding monotonic test and, at the same displacement level, subsequent cycles exhibit load decay.

To account for these two phenomena the following parameters could be defined:

$$\alpha_{N,1} = \frac{N_{um,cyc,1}}{N_{um,mon}} \tag{6}$$

where $N_{um,cyc,1}$ is the mean peak resistance at the first cycle, evaluated as

$$N_{um,cyc,1} = \frac{1}{n} \bullet \sum_{i=1}^{n} N_{u,cyc,1,i}$$

being $N_{u,cyc,1,i}$ the peak resistance in the test *i*, and $N_{um,mon}$ the mean peak resistance calculated from the monotonic reference tests, and

$$\alpha_{N,2} = \frac{N_{um,cyc,3}}{N_{um,cyc,1}} \tag{7}$$

Table 4
- α_{seis} coefficients.

Diameter/ Position	8 M	8 TJ	10 M	10 TJ	12 M	12 TJ	12 M*	12 TJ*
$\alpha_{seis,1}$	0.96	0.67	0.95	0.70	1	0.74	0.94	0.99
$\alpha_{seis,3}$	0.78	0.73	0.84	0.76	0.78	0.79	0.81	0.83
α_{seis}	**0.74**	**0.49**	**0.80**	**0.53**	**0.78**	**0.58**	**0.76**	**0.83**

*Evaluated in cyclic tests with residual displacement.

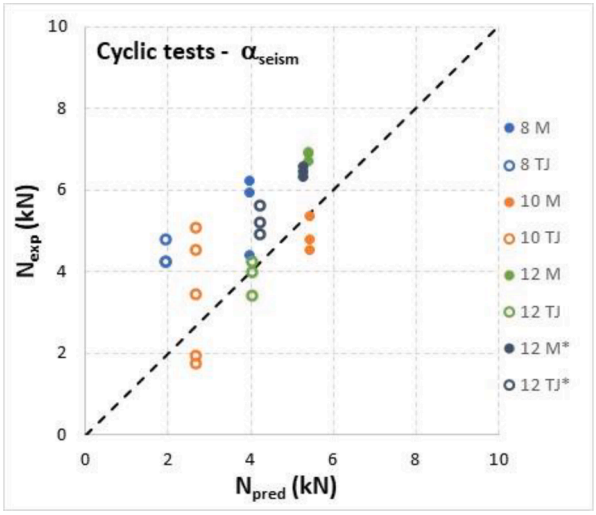

Fig. 22. Experimental/predicted load ratio of cyclic tests considering α_{seis}.

where $N_{um,cyc,3}$ is the mean peak resistance at the third cycle (assessment analogue to $N_{um,cyc,1}$).

The final reduction factor can be defined as: $\alpha_{seis} = \alpha_{N,1} \bullet \alpha_{N,2}$.

The α_{seis}-coefficients evaluated based on the experimental results are reported in Table 4. In general, the α_{seis}-values in the T-joint (from 0.49 to 0.58) are significantly lower than in the brick locations (from 0.74 to 0.80). This is due to a larger reduction coming from the ultimate load ratio $\alpha_{N,1}$, whereby the cyclic tests with residual displacement (diameter 12) did not show this effect.

By multiplying the predicted load by the α_{seis} coefficient, the results

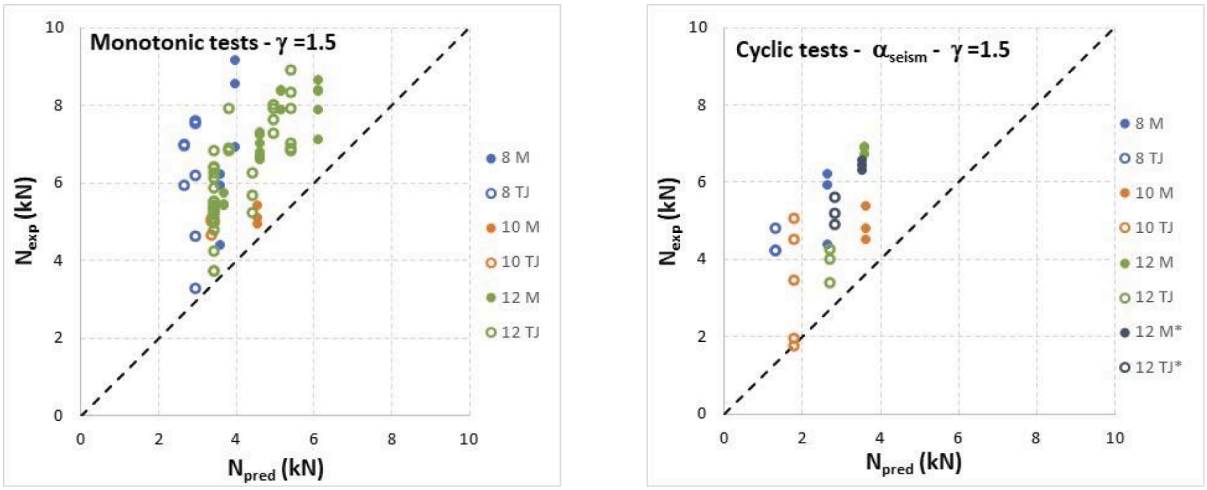

Fig. 23. Experimental/predicted load ratio with a safety factor of 1.5 applied on the predicted load for monotonic (a) and cyclic (b) tests.

reported in Fig. 22 are obtained.

In summary, on a mean basis, the results are sufficiently well predicted by the approach with a tendency for conservative values except for diameter 10 (which exhibits high scatter in particular in the T-joint) and diameter 12 in the T-joint without residual displacement.

Nevertheless, the obtained values are just the prediction of the mean experimental results, thus for design purposes the characteristic resistances should be evaluated and the safety factor γ_M should be applied (EAD 330,284 or EAD 330076 for masonry recommend $\gamma_M = 2.5$ for base material related failure modes, the latter even for seismic actions). The coefficients of variation measured in the experimental campaign were reasonably low, thus the reduction of load from average values to characteristic values is expected to be limited, while the safety factor will dramatically reduce the final design load. Indeed, as an example, by simply considering a safety factor of 1.5 (Fig. 23), all data lies in the safe side domain, suggesting that the value of 2.5 is too conservative.

In summary, it can be concluded that the proposed equation (3) is able to predict the expected failure load with sufficient accuracy. Nevertheless, the equation includes the base material strength, that in the present study was evaluated on the basis of actual material strength and the location of the connection (TJ or M).

On jobsite, the evaluation of the base material compressive strength is challenging, and the uncertainty of the results is assumed high. Thus, to properly apply Eq. (3), it is suggested to conduct jobsite tension tests (series of minimum 5 replicates with embedment length 200 mm, diameter 12 mm) and to back-evaluate the base material strength (f_{bm}) of the considered wall or building from Eq. (3). Once this parameter is defined, Eq. (3) can be used to predict the different connection configurations (embedment length, diameter…).

5. Conclusions

An experimental campaign on the tensile behavior of twisted stainless steel bars Hilti Heli-Brick considering different parameters (bar diameter, the embedment depth, position within the wall, strength of the masonry and the type of loading) was conducted. Based on the experimental results the following considerations can be drawn:

- Overall twisted stainless-steel bars showed very good performance with reliable results associated to low coefficient of variation of the loads and with a very limited damage of the base material.
- The load–displacement curves revealed a good ductility, an excellent agreement between monotonic and cyclic tests, with an extended plateau for brick locations and a limited plateau in the case of installation in the mortar joints.
- By increasing the embedment length beyond 100 mm, the load increases but not proportionally.
- Indeed, beside the embedment depth, the position within the wall and the wall types (weak/ strong) were the most influential parameters, with higher loads associated to the location of the bar in middle of the brick. Overall soft and weak materials lead to lower load and to a more brittle behavior than stiff and strong materials.
- There is no clear correlation between ultimate load and the bar diameter. This is ascribed to the differences in the bar geometry (e.g., cross-section and pitch) and corresponding diameter of the borehole (undercut and interaction with bar core).
- Overall, response under cyclic load and under monotonic load were similar, although some degradation was observed.
- The equation proposed to evaluate the maximum load depends on the geometrical characteristics of the bar, borehole diameter and on the strength of the masonry. For practical cases the latter parameter should be evaluated via job-site tension testing.
- For applications under seismic actions, in the calculation of the resistances, reduction factors in the style of the existing EAD 330076-v01 should be considered to account for degradation effects resulting from cyclic loading.

CRediT authorship contribution statement

Sara Cattaneo: Conceptualization, Data curation, Investigation, Methodology, Project administration, Supervision, Writing – original draft. **Manuela Scamardo:** Formal analysis, Investigation, Data curation, Validation, Writing – review & editing, Visualization.

Declaration of Competing Interest

The authors declare that they have no known competing financial interests or personal relationships that could have appeared to influence the work reported in this paper.

Data availability

The authors do not have permission to share data.

Acknowledgments

While opinions, findings, and conclusions are those of the authors, we would like to thank Dr. Georg Welz for his insights, expertise and suggestions throughout the preparation and review of this article, together with the technical staff of the Materials and Structures Testing Laboratory of Politecnico di Milano (particularly, Mr. Daniele Spinelli and Roberto Minerva) for their assistance during the experimental work.

References

[1] A. Penna, P. Morandi, M. Rota, C.F. Manzini, F. da Porto, G. Magenes, Performance of Masonry Buildings during the Emilia 2012 Earthquake, Bull. Earthq. Eng. 12 (5) (2014) 2255–2273.
[2] G. Vlachakis, E. Vlachaki, P.B. Lourenço, Learning from Failure: Damage and Failure of Masonry Structures, after the, Lesvos Earthquake (Greece), Eng. Fail. Anal. 2020 (2017) 117.
[3] R.K. Adhikari, D. D'Ayala, Nepal Earthquake: Seismic Performance and Post-Earthquake Reconstruction of Stone in Mud Mortar Masonry Buildings, Bull. Earthq. Eng. 18 (8) (2020) 3863–3896.
[4] S. Bhattacharya, S. Nayak, S.C. Dutta, A critical review of retrofitting methods for unreinforced masonry structures, Int. J. Disaster Risk Reduct. 7 (2014) 51–67.
[5] R. Capozucca, E. Magagnini, Experimental response of masonry walls in-plane loading strengthened with GFRP strips, Compos. Struct. 235 (2020).
[6] N. Longarini, P. Crespi, M. Scamardo, Numerical approaches for cross-laminated timber roof structure optimization in seismic retrofitting of a historical masonry church, Bull. Earthq. Eng. 18 (2) (2020) 487–512.
[7] M. Scamardo, P. Crespi, N. Longarini, M. Zucca, Seismic vulnerability and retrofitting of a historical masonry building, 9th Euro-American Congress on Construction Pathology, Rehabilitation Technology and Heritage Management, REHABEND 2022 Granada, Pages 787 – 7942022.
[8] M. ElGawady, P. Lestuzzi, M. Badoux. Retrofitting of Masonry Walls Using Shotcrete. 2006 NZSEE Conference (2006) 45–54.
[9] J.A.P.P. Almeida, E.B. Pereira, J.A.O. Barros, Assessment of Overlay Masonry Strengthening System under In-Plane Monotonic and Cyclic Loading Using the Diagonal Tensile Test, Constr. Build. Mater. 94 (2015) 851–865.
[10] L. Biolzi, S. Cattaneo, P. Crespi, M. Scamardo, N. Vafa, Diagonal compression cyclic testing of unreinforced and reinforced masonry walls, Constr. Build. Mater. 363 (2023) art. no. 129839.
[11] M. Scamardo, S. Cattaneo, L. Biolzi, N. Vafa, Parametric Analyses of the Response of Masonry Walls with Reinforced Plaster, Applied Sciences (Switzerland) (2022), 12.
[12] F. Yavartanoo, T.-K. Kang, Retrofitting of Unreinforced Masonry Structures and Considerations for Heritage-Sensitive Constructions, J. Build. Eng. 49 (2022).
[13] S. Paganoni, D. D'Ayala, Testing and design procedure for corner connections of masonry heritage buildings strengthened by metallic grouted anchors, Eng. Struct. 70 (2014) 278–293.
[14] A. Cascardi, M. Leone, M.A. Aiello, Transversal joining of multi-leaf masonry through different types of connector: Experimental and theoretical investigation, Constr. Build. Mater. 265 (2020).
[15] S. Cattaneo, N. Vafa, Tensile capacity of adhesive anchors in damaged masonry, Appl. Sci. 11 (21) (2021) 10135.
[16] S. Moreira, L.F. Ramos, B. Csikai, P. Bastos, Bond behavior of twisted stainless-steel bars in mortar joints, In International Conference Proceedings on 9th International Masonry Conference, 2014.
[17] C. Gentilini, F. Finelli, V.A. Girelli, E. Franzoni, Pull-out behavior of twisted steel connectors employed in masonry: the influence of the substrate, Constr. Build. Mater. 274 (2021) art. no. 122115.
[18] C. Gentilini, F. Finelli, C. Carloni, An experimental study of the bond behavior of twisted steel bars embedded in mortar cylinders and in the joints of masonry wallettes, Constr. Build. Mater.316 (2022) art. no. 125795.
[19] R.B. Petersen, N. Ismail, M.J. Masia, J.M. Ingham, Finite element modelling of unreinforced masonry shear wallets strengthened using twisted steel bars, Constr. Build. Mater. 33 (2012) (2012) 14–24.
[20] S. Cattaneo, P. Crespi, M. Scamardo, Heli-brick experimental assessment, Internal Report Dept. ABC – Politecnico di Milano 9/2022.
[21] Hilti Heli-Brick documentation and instructions for use, Hilti Italia S.p.A.
[22] CEN, EN 772-1:2015, Methods of test for masonry units. Determination of compressive strength.
[23] CEN, EN 1015-11:2019 Methods of test for mortar for masonry. Determination of flexural and compressive strength of hardened mortar.
[24] S. Cattaneo, A. Locatelli, D. Rago, Reliability of bonded anchors with different installation techniques: Experimental assessment, Asian J. Civil Eng. 20 (5) (2019) 681–692.
[25] D.M. 20/11/1987, Norme tecnica per la progettazione, esecuzione e collaudo degli edifici in muratura e per il loro consolidamento, Italian Ministry of infrastructures.
[26] EAD 330076-01-0604-v01: Metal injection anchors for use in masonry under seismic actions. EOTA, Brussels, Belgium, May 2022.